Improved Murine MHC-Deficient HLA Transgenic NOD Mouse Models for Type 1 Diabetes Therapy Development

Jeremy J. Racine,[1] Isabel Stewart,[1] Jeremy Ratiu,[1] Greg Christianson,[1] Emily Lowell,[1] Kelsay Helm,[1] Jennifer Allocco,[1] Richard S. Maser,[1] Yi-Guang Chen,[2] Cathleen M. Lutz,[1] Derry Roopenian,[1] Jennifer Schloss,[3] Teresa P. DiLorenzo,[3] and David V. Serreze[1]

Diabetes 2018;67:923–935 | https://doi.org/10.2337/db17-1467

Improved mouse models for type 1 diabetes (T1D) therapy development are needed. T1D susceptibility is restored to normally resistant NOD.β2m$^{-/-}$ mice transgenically expressing human disease–associated HLA-A*02:01 or HLA-B*39:06 class I molecules in place of their murine counterparts. T1D is dependent on pathogenic CD8$^+$ T-cell responses mediated by these human class I variants. NOD.β2m$^{-/-}$-A2.1 mice were previously used to identify β-cell autoantigens presented by this human class I variant to pathogenic CD8$^+$ T cells and for testing therapies to attenuate such effectors. However, NOD.β2m$^{-/-}$ mice also lack nonclassical MHC I family members, including FcRn, required for antigen presentation, and maintenance of serum IgG and albumin, precluding therapies dependent on these molecules. Hence, we used CRISPR/Cas9 to directly ablate the NOD H2-K^d and H2-D^b classical class I variants either individually or in tandem (cMHCI$^{-/-}$). Ablation of the H2-A^{g7} class II variant in the latter stock created NOD mice totally lacking in classical murine MHC expression (cMHCI/II$^{-/-}$). NOD-cMHCI$^{-/-}$ mice retained nonclassical MHC I molecule expression and FcRn activity. Transgenic expression of HLA-A2 or -B39 restored pathogenic CD8$^+$ T-cell development and T1D susceptibility to NOD-cMHCI$^{-/-}$ mice. These next-generation HLA-humanized NOD models may provide improved platforms for T1D therapy development.

The study of NOD mice has greatly advanced knowledge of the genetics and pathogenic mechanisms underlying autoimmune-mediated type 1 diabetes (T1D) (1). However, as a model for translating this knowledge into clinically applicable therapies, NOD mice have been less successful (2). A potential way to improve NOD as a preclinical platform is to "humanize" the strain with a variety of genes relevant to T1D patients (3,4). A desired humanization process would turn an inbred mouse potentially representing one T1D patient profile, into a multiplex platform capable of representing an array of such individuals. Such pipeline models could be used to test therapies with potential efficacy in heterogeneous at-risk T1D subjects.

While polygenic in nature, specific MHC (designated HLA in humans) haplotypes provide the strongest T1D risk factor (5,6). Hence, a flexible panel of HLA-"humanized" NOD mice may provide improved models for testing potentially clinically applicable T1D interventions. In humans, particular HLA class II variants, such as DQ8 and DR3/4, mediating autoreactive CD4$^+$ T-cell responses strongly contribute to T1D susceptibility (7–9). Similarly, the murine H2-A^{g7} class II variant, highly homologous with the human DQ8 molecule, is a primary T1D contributor in NOD mice (10). However, findings that NOD mice made deficient in MHC class I expression and CD8$^+$ T cells by introduction of an inactivated *β2m* allele (NOD.β2m$^{-/-}$) are completely T1D resistant (11) indicated that this immunological arm is also critical to disease development. It was subsequently found that particular HLA class I variants also contribute to T1D susceptibility in patients (12–16). Thus, a desirable pipeline model system would enable generation of NOD mice expressing chosen combinations of human T1D–associated HLA class I and II variants in the absence of their murine counterparts that could then serve to test potential clinically relevant disease interventions.

T1D-associated class I susceptibility variants in humans include HLA-A*02:01 (hereafter HLA-A2.1) and HLA-B*39:06

[1]The Jackson Laboratory, Bar Harbor, ME
[2]Medical College of Wisconsin, Milwaukee, WI
[3]Albert Einstein College of Medicine, Bronx, NY
Corresponding author: David V. Serreze, dave.serreze@jax.org.

Received 4 December 2017 and accepted 12 February 2018.

This article contains Supplementary Data online at http://diabetes.diabetesjournals.org/lookup/suppl/doi:10.2337/db17-1467/-/DC1.

(hereafter HLA-B39) (12–19). HLA-A2 is in strong linkage disequilibrium with the DR4/DQ8 class II haplotype, the primary contributor to T1D development in Caucasians (14). Hence, the A2 class I variant will be present in the preponderance of T1D patients. While representing a relatively low frequency allele, the B39 variant supports aggressive early-age-of-onset T1D development (15,16). The original HHD transgene construct contains the genomic promoter and first three exons of HLA-A*02:01, encoding the antigen-presenting α1 and α2 domains, as well as a covalently linked human β2m with the α3, transmembrane, and cytoplasmic domains of murine H2-D^b origin, allowing for proper signaling within mice (20). When introduced into normally disease-resistant NOD.β2m$^{-/-}$ mice, HHD transgene expression of HLA-A2.1 in the absence of any murine class I molecules restored the generation of pathogenic CD8$^+$ T cells mediating insulitis and T1D development (21). These mice allowed identification of HLA-A2.1–restricted autoantigenic epitopes derived from the pancreatic β-cell proteins insulin and IGRP (21–23) also targeted by CD8$^+$ T cells from human patients expressing this class I variant (24–29). This subsequently led to development of some proof-of-principle antigen-specific therapeutics (30). The B39 variant appears to be a highly potent human T1D contributory class I molecule, particularly in terms of promoting early-age disease onset (12,17–19). Introduction of a modified HHD transgene cassette, in the absence of murine class I molecules, induced expression of the α1 and α2 domains of B39, rather than A2, with the rest of the construct remaining as originally described (20), and also restored generation of T1D-inducing CD8$^+$ T cells in NOD.β2m$^{-/-}$ mice (31). These previous findings illustrate the potential of having patient-derived models for testing possible T1D therapies.

The first-generation HLA-A2 and -B39 transgenics required pairing with the β2m$^{-/-}$ mutation to eliminate murine MHC I expression. While β2m$^{-/-}$ mice lack expression of the classical murine H2-D and H2-K MHC class I molecules, this mutation additionally ablates nonclassical MHC molecules such as CD1d and Qa-2, potentially altering immune processes. β2m$^{-/-}$ mice also lack expression of FcRn, a nonclassical MHC I molecule critical for serum IgG and albumin homeostasis pathways including processing and presentation of IgG complexed antigens to T cells (32–35). Hence, β2m$^{-/-}$ NOD mouse models are not suited for investigating potential antibody- or serum albumin–based (36) T1D interventions. To overcome these hurdles, we used clustered regularly interspaced short palindromic repeats (CRISPR)-associated endonuclease (Cas)9 technologies to generate novel NOD stocks in which the classical *H2-K1*^{d} and *H2-D1*^{b} class I genes were directly ablated individually or in tandem (respectively designated NOD-H2-K$^{-/-}$, NOD-H2-D$^{-/-}$, and NOD-cMHCI$^{-/-}$). We then genetically eliminated the H2-A^{g7} class II variant in NOD-cMHCI$^{-/-}$ mice, resulting in a strain fully lacking classical murine MHC molecules (NOD-cMHCI/II$^{-/-}$). These strains retain β2m-dependent FcRn activity and can be used as platforms for the introduction of selected combinations of HLA class I and II variants relevant to T1D patients. As a first step in validating such second-generation HLA-humanized models, we report that HLA-A2– or HLA-B39–encoding HHD transgenes support development of T1D-inducing CD8$^+$ T cells in such strains.

RESEARCH DESIGN AND METHODS

Mice: General

NOD/ShiLtDvs (hereafter NOD) and all other mouse strains described herein are maintained at The Jackson Laboratory under specific pathogen-free conditions. NOD-Tg(HLA-A/H2-D/B2M)1Dvs/Dvs (commonly called NOD-HHD [hereafter NOD-A2]), NOD.129P2(B6)-B2m^{tm1Unc} Tg(HLA-A/H2-D/B2M)1Dvs/Dvs (hereafter NOD.β2m$^{-/-}$-A2), NOD.129P2(B6)-B2m^{tm1Unc} (hereafter NOD.β2m$^{-/-}$), and NOD.Tg(HLA-B39/H2-D/B2M)2Dvs/Dvs (hereafter NOD-B39) have previously been described (11,21,31).

Mouse Model Development

NOD zygotes were injected with 100 ng/μL *Cas9* mRNA and 50 ng/μL single guide RNA containing specific guide sequences for the targeted gene (described in more detail in the figure legends). Mosaic founders were crossed back to the NOD background for at least one generation, and resulting offspring were analyzed for mutations using the procedures detailed below.

Genotyping NOD-H2-D$^{-/-}$

PCR amplification of exon 1 and 2 of *H2-D1*^{b} was performed with batch 1 (forward primer 5′-TCAGACACCCGGGATCCCAGATGG-3′, and reverse primer 5′-CGCGCTCTGGTTGTAGTAGCCGAG-3′) or batch 2 (forward primer 5′-GGCGAGATTCCAGGAGCCAA-3′ and reverse primer 5′-TTCCGGGTCCGTTCTGTTCC-3′). Sequencing for batch 1 was performed with reverse primer 5′-CAGGTTCCTCAGGCTCACTC-3′ or 5′-TTTCCCGCTCCCAATACTC-3′. Sequencing primer for batch 2 was performed either with the two reverse sequencing primers from batch 1 or with batch 1's forward primer. Zygosity was determined by restriction-length polymorphisms using the above batch 2 primers, as the mutation described herein disrupts an *Xho*I restriction site within exon 2 (data not shown).

Genotyping NOD-H2-K$^{-/-}$

PCR amplification of exons 2 and 3 of *H2-K1*^{d} was performed using forward primer 5′-ATTCGCTGAGGTATTTCGTC-3′ and reverse primer 5′-TTCTCTCCTTCCCTCCTGAGAC-3′. Sequencing was performed using forward primer 5′-CCCGGAACCGGTTTCCCTTT-3′. Homozygosity was confirmed by flow cytometry, showing a lack of H2-K expression on blood B cells.

Genotyping NOD-cMHCI$^{-/-}$

Sequencing of *H2-D1*^{b} was performed as described above. For sequencing of *H2-K1*^{d}, a PCR product spanning most of exons 1 and 2 was amplified using forward primer 5′-AGTCGCTAATCGCCGACCAGT-3′ and reverse primer 5′-CGGGAAGTGGAGGGGTCGTG-3′. These primers were also used

for sequencing. Homozygosity was additionally typed by flow cytometry analysis of peripheral blood $B220^+$ cells, showing a lack of H2-K and H2-D.

NOD-cMHCI$^{-/-}$-A2 and NOD-cMHCI$^{-/-}$-B39

NOD-A2 or NOD-B39 mice were crossed to NOD-cMHCI$^{-/-}$ mice. Resulting offspring were backcrossed to NOD-A2 or NOD-B39 mice. Offspring were selected for homozygosity of A2 or B39 transgenes. For quantitative PCR analysis of the B39 transgene, forward primer 5′-GGAGACACGGAAAGTGAAGG-3′, reverse primer 5′-GGCCTCGCTCTGGTTGTAG-3′, and transgene probe 5′-6-FAM-CCGAGTGGACCTGGGGACCC-Black Hole Quencher 1, 3′ were used. Internal control forward primer 5′-CACGTGGGCTCCAGCATT-3′, reverse primer 5′-TCACCAGTCATTTCTGCCTTTG-3′, and control probe 5′-Cy5-CCAATGGTCGGGCACTGCTCAA-Black Hole Quencher 2, 3′ were also used. The specific quantitative PCR conditions for the HHD transgene are publically available online for NOD-A2 mice (JAX strain 006604). Samples were run on a LightCycler 480 System (F. Hoffman-LaRoche Ltd). *H2-D1* sequencing analysis as described above was used to identify MHCI$^{+/-}$ mice, which were then intercrossed to fix MHCI$^{-/-}$ mutations, and homozygosity was determined by flow cytometry analysis of peripheral blood $B220^+$ cells, showing a lack of H2-K and H2-D.

Genotyping NOD-cMHCI/II$^{-/-}$

For sequencing of *H2-Ab1*^{g7}, a PCR product spanning exon 2 was amplified using the forward primer 5′-CATCCCTCCCTTGCTCTTCCTTAC-3′ and reverse primer 5′-TGAGGTCACAGCAGAGCCAG-3′. The same forward primer was used for sequencing this PCR product. Mice were additionally genotyped by amplification length polymorphisms (data not shown).

Sequencing

PCR products were amplified as described for each strain above (and Supplementary Figs. 1 and 4) and then purified and analyzed by sequencing on the 3730 DNA Analyzer (Applied Biosystems, Inc.). Mutant sequences were separated from wild type using the Poly Peak Parser package (37) for R.

Flow Cytometry

Single-cell leukocyte suspensions were stained and run on an LSRII SORP (BD Biosciences), Attune Acoustic Focusing Cytometer (Thermo Fisher Scientific), or FACSAria II (BD Biosciences), with all analyses performed using FlowJo 10 (FlowJo, LLC). For splenic samples, single-cell suspensions were lysed with Gey's buffer to remove red blood cells (38). Doublet discrimination was performed (forward scatter A [FSC-A] vs. FSC-H with additional side scatter A vs. side scatter H gating for LSRII or SORP and FACSAria II panels) and live/dead discrimination assessed via propidium iodide staining. The following monoclonal antibodies were used: from BD Biosciences, H-2K^d (SF1-1.1), B220 (RA3-6B2), CD8α (53-6.7), CD4 (GK1.5 and RM4-5), CD62L (MEL-14), CD44 (IM7.8.1), CD19 (1D3), CD45.1 (A201.7), CD90.2 (53–2.1), H-2D^b (KH95), and I-A^d (AMS-32.1); from BioLegend, H-2L^d/H-2D^b (28-14-8), H-2D^b (KH95), HLA-A,B,C (W6/32), CD8α (53-6.7), CD4 (GK1.5), Qa-2 (695H1-9-9), CD1d (1B1), CD90.2 (30-H12), and T-cell receptor (TCR)γδ (GL3). HLA-A2.1–specific monoclonal antibody CR11-351 (21,39) was also used. Mouse PBS-57:CD1d tetramer (hereafter CD1d-α-GalCer tetramer) was obtained from the National Institutes of Health Tetramer Facility.

Monitoring T1D Development

Ames Diastix (Bayer) were used to assess glycosuria weekly. T1D onset was defined by two readings of ≥0.25% (≥300 mg/dL in blood) on two separate days.

Insulitis Scoring

Mean insulitis scores were determined as previously described using a 0 (no visible lesions) to 4 (75–100% islet destruction) scoring method (40).

Islet-Associated Leukocyte Isolation

Islet-infiltrating leukocyte populations were isolated for flow cytometry as previously described (41).

Antibody Pharmacokinetic Study

Herceptin was detected from plasma samples using a human IgG ELISA kit according to the manufacturer's instructions (Mabtech). Trinitrophenol/dinitrophenol cross-reactive IgG1 antibody 1B7.11 was detected from plasma samples by capturing with dinitrophenol-BSA (Calbiochem) coated onto ELISA plates (Costar) at 0.5 μg/mL PBS, blocked with 1% BSA in PBS + 0.05% Tween 20, and detected with goat anti-mouse κ-alkaline phosphatase (Southern Biotech).

Statistical Analysis

Prism 6 (GraphPad) was used to generate all graphs and statistics. All *P* values for scatter dot plots are from two-tailed Mann-Whitney analyses. All *P* values for diabetes incidence studies were calculated by Mantel-Cox analysis.

RESULTS

Creation of Novel NOD-H2-D$^{-/-}$ and NOD-H2-K$^{-/-}$ Mice

We previously generated, through combined use of the $\beta 2m^{-/-}$ mutation and HHD-based transgenes, murine MHC class I–deficient NOD mouse stocks expressing human HLA-A*02:01 (A2) or HLA-B*39:06 (B39) counterparts capable of supporting diabetogenic $CD8^+$ T-cell responses (4,30,31). However, the $\beta 2m^{-/-}$ mutation also ablates expression of nonclassical class I molecules including CD1d or Qa-2 (Fig. 1*A* and *B*) and FcRn. Thus, the $\beta 2m^{-/-}$ mutation negatively impacts the ability to evaluate possible T1D interventions whose activities require nonclassical MHCI/β2m protein complexes. For this reason, we created new direct-in-NOD (as opposed to congenic transfer of mutations) MHC I knockout models to improve upon the first-generation HLA-humanized mice. We further envisioned that these novel stocks would provide a means to understand the independent contributions of the K^d and D^b classical class I alleles to T1D pathogenesis in NOD mice. Initially, NOD-H2-D$^{-/-}$ mice were generated using CRISPR/Cas9 to target exon 2 of *H2-D1*^{b}. Four resultant lines were bred to homozygosity

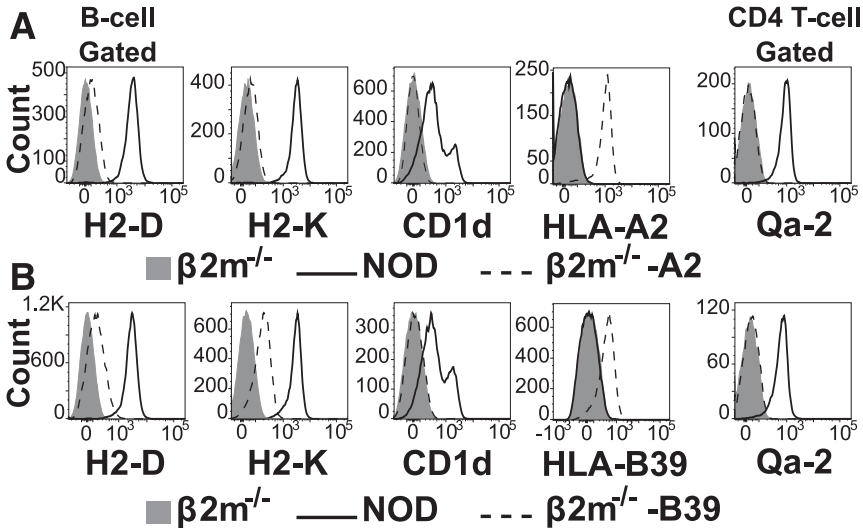

Figure 1—HLA-humanized NOD mice lack both classical and nonclassical MHC I molecules. *A* and *B*: Representative histograms showing splenic B-cell expression of H2-D, H2-K, CD1d, transgenic human HLA class I, or splenic CD4$^+$ T-cell expression of Qa-2 comparing NOD and β2m$^{-/-}$ controls with NOD.β2m$^{-/-}$-A2 (*A*) or NOD.β2m$^{-/-}$-B39 (*B*) mice.

(Fig. 2*A* and data not shown). An NOD-H2-D$^{-/-}$ line carrying a single nucleotide deletion within exon 2 (Fig. 2*A*) was chosen for in-depth analysis based on breeding proclivity. As expected, B220$^+$ splenocytes (and other populations [Supplementary Fig. 2]) from NOD-H2-D$^{-/-}$ mice lack H2-D but retain H2-K expression (Fig. 2*B* and *C*). There are no obvious perturbations of thymic populations based on frequency (Fig. 2*D* and *E*) or yield (Fig. 2*F*). However, there is a subtle shift in the percentage of CD8$^+$ T cells in the spleen and pancreatic lymph node (PancLN) (Fig. 2*G* and *H*). This shift, however, did not correspond with any changes in the yield of either CD4$^+$ or CD8$^+$ T cells in spleens or PancLNs (Fig. 2*I*).

Next, we generated NOD-H2-K$^{-/-}$ mice using CRISPR/Cas9 to target exon 3 of *H2-K1^d*. A line carrying a two–base pair (bp) deletion within exon 3 (Fig. 3*A*) was chosen for in-depth analysis based on breeding proclivity. As expected, NOD-H2-K$^{-/-}$ mice lack H2-K but retain H2-D expression (Fig. 3*B* and *C* and Supplementary Fig. 2). In contrast to the NOD-H2-D$^{-/-}$ stock (Fig. 2*D* and *E*), NOD-H2-K$^{-/-}$ mice showed a small but significant percentage increase in double-positive and a reduction in CD8$^+$ single-positive thymocytes (Fig. 3*D* and *E*) that did not translate to thymic yields (Fig. 3*F*). However, a more robust change in splenic and PancLN CD8$^+$ T-cell percentage (Fig. 3*G* and *H*) was observed than in H2-D$^{-/-}$ mice (Fig. 2*G* and *H*), leading to a drastic reduction in CD8$^+$ T cells in both organs, along with a slight rise in splenic CD4$^+$ T-cell yields (Fig. 3*I*).

Having generated H2-D$^{-/-}$ and H2-K$^{-/-}$ NOD mice, we assessed the individual contributions of these variants to T1D development. Both NOD-H2-D$^{-/-}$ and NOD-H2-K$^{-/-}$ mice had significantly delayed and reduced T1D development compared with standard NOD controls but did not significantly differ from one another (Fig. 4*A*). Prior to their cryopreservation, several additional H2-D and H2-K knockout lines were assessed for T1D incidence, showing similar kinetics and penetrance (Supplementary Fig. 1A and *B*). Additionally, compared with NOD controls, insulitis was decreased in both NOD-H2-D$^{-/-}$ and NOD-H2-K$^{-/-}$ mice at 10–15 weeks of age, as well as at the end of incidence, with no differences between the two groups (Fig. 4*B* and *C*).

We next examined the makeup of islet-infiltrating CD8$^+$ T cells in NOD-H2-D$^{-/-}$ and NOD-H2-K$^{-/-}$ mice. Among islet-infiltrating leukocytes, we found no difference in the percentage of T cells between NOD and the two knockout lines (Fig. 4*D* and *E*). Interestingly, NOD-H2-D$^{-/-}$ mice had frequencies of CD8$^+$ T cells among islet-infiltrating T cells similar to those in NOD controls (Fig. 4*D–F*). NOD-H2K$^{-/-}$ mice, however, had reduced and increased percentages of CD8$^+$ and CD4$^+$ T cells, respectively, compared with both NOD and NOD-H2-D$^{-/-}$ mice. Unexpectedly, the frequencies of CD44$^+$ CD62L$^-$ effector CD8$^+$ T cells but not CD44$^+$ CD62L$^+$ central memory T cells were increased in NOD-H2-K$^{-/-}$ mice compared with both NOD and NOD-H2-D$^{-/-}$ mice, with a concomitant reduction of CD44$^-$ CD62L$^+$–naïve cells (Fig. 4*G*).

Creation of NOD-cMHCI$^{-/-}$ Mice

We next simultaneously targeted *H2-D1^b* and *H2-K1^d* to generate NOD mice directly lacking expression of both classical murine MHC class I molecules. Three founders were generated carrying predicted frameshift mutations within exon 2 of *H2-D1^b* and *H2-K1^d* (Fig. 5*A* and data not shown). Based on breeding proclivity, we selected an NOD-cMHCI$^{-/-}$ line carrying spaced 11- and 3-bp deletions within *H2-D1* and a 1-bp deletion in *H2-K1* (Fig. 5*A*) for analyses. As expected, these NOD-cMHCI$^{-/-}$ mice lack H2-D and H2-K (Fig. 5*B* and Supplementary Fig. 2). This lack of MHC I expression corresponded with a paucity of splenic CD8$^+$ TCRβ$^+$ cells (Fig. 5*C* and *D*). Due to the ability of the NOD-cMHCI$^{-/-}$ stock to express nonclassical MHC Ib molecules,

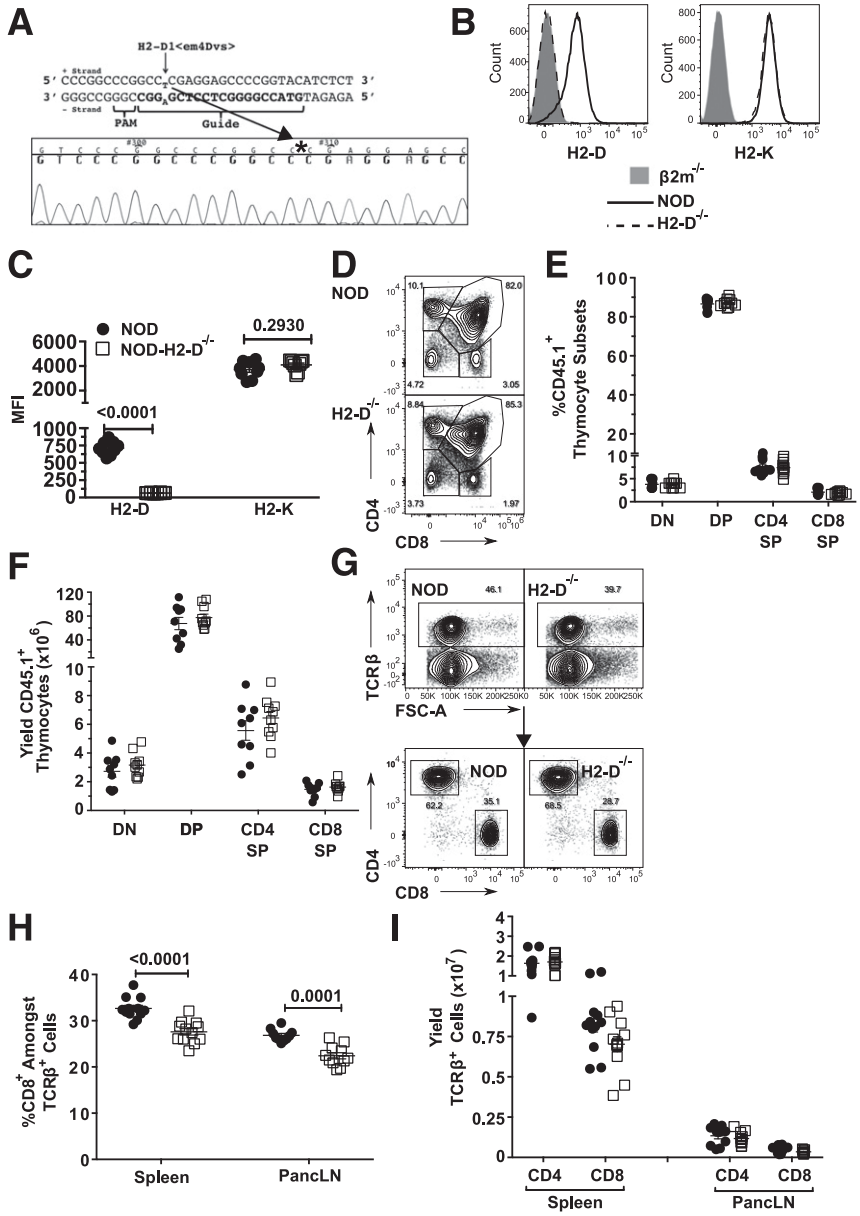

Figure 2—Novel direct-in-NOD H2-D knockout mouse generated with CRISPR/Cas9. *A*: Diagram (top) and sequence trace (bottom) showing guide sequence (boldface type) and protospacer adjacent motif (PAM) site within exon 2 of *H2-D1*^{b} used to generated NOD-H2-D$^{-/-}$ mice (officially designated NOD/ShiLtDvs-H2-D1$^{<em4Dvs>}$/Dvs). The subscript nucleotide represents the H2-D1<em4Dvs> mutation that is denoted with an asterisk on the sequence trace where that nucleotide is missing. *B*: Representative flow cytometry histogram showing expression of H2-D and H2-K antibody staining on the surface of splenic B cells in comparison of 10-week-old female NOD, NOD.β2m$^{-/-}$, and NOD-H2-D$^{-/-}$ mice. *C*: Quantification of the mean fluorescence intensity (MFI) of H2-D and H2-K antibody staining on splenic B cells (showing mean ± SEM). *D*: Representative flow cytometry showing CD4 vs. CD8 of gated CD45.1^{+} thymocytes in comparison of 10-week-old female NOD and NOD-H2-D$^{-/-}$ mice. *E* and *F*: Quantification of percentage (*E*) and yield (*F*) of CD45.1^{+} thymic subsets (DN, double negative; DP, double positive; SP, single positive) (showing mean ± SEM). *G*: Representative flow cytometry showing among splenocytes TCRβ vs. FSC-A (top) and TCRβ-gated CD4 vs. CD8 (bottom) from 10-week-old female mice. *H* and *I*: Percent CD8^{+} among TCRβ-gated cells (*H*) and yield (*I*) of spleen and PancLN CD4^{+} and CD8^{+} T cells (showing mean ± SEM). All scatterplots plot individual mice (9–16 mice per group per analysis) pooled from two to three experiments.

they were characterized by small, but significant, increase in the yield of splenic CD8^{+} T cells compared with NOD.β2m$^{-/-}$ mice (Fig. 5*C* and *D*). Compared with standard NOD controls, both NOD-cMHCI$^{-/-}$ and NOD.β2m$^{-/-}$ mice had increased CD4^{+} yields, with this elevation greatest in the latter stock (Fig. 5*D*). Similar to NOD.β2m$^{-/-}$ mice, NOD-cMHCI$^{-/-}$ mice were resistant to T1D (Fig. 5*E* and Supplementary Fig. 1C) and insulitis out to 30 weeks of age (Fig. 5*F*).

Second-Generation NOD-cMHCI$^{-/-}$-A2 and NOD-cMHCI$^{-/-}$-B39 Mice

To test whether it could be used as a new base model for HLA "humanization" in lieu of stocks carrying the *β2m*$^{-/-}$

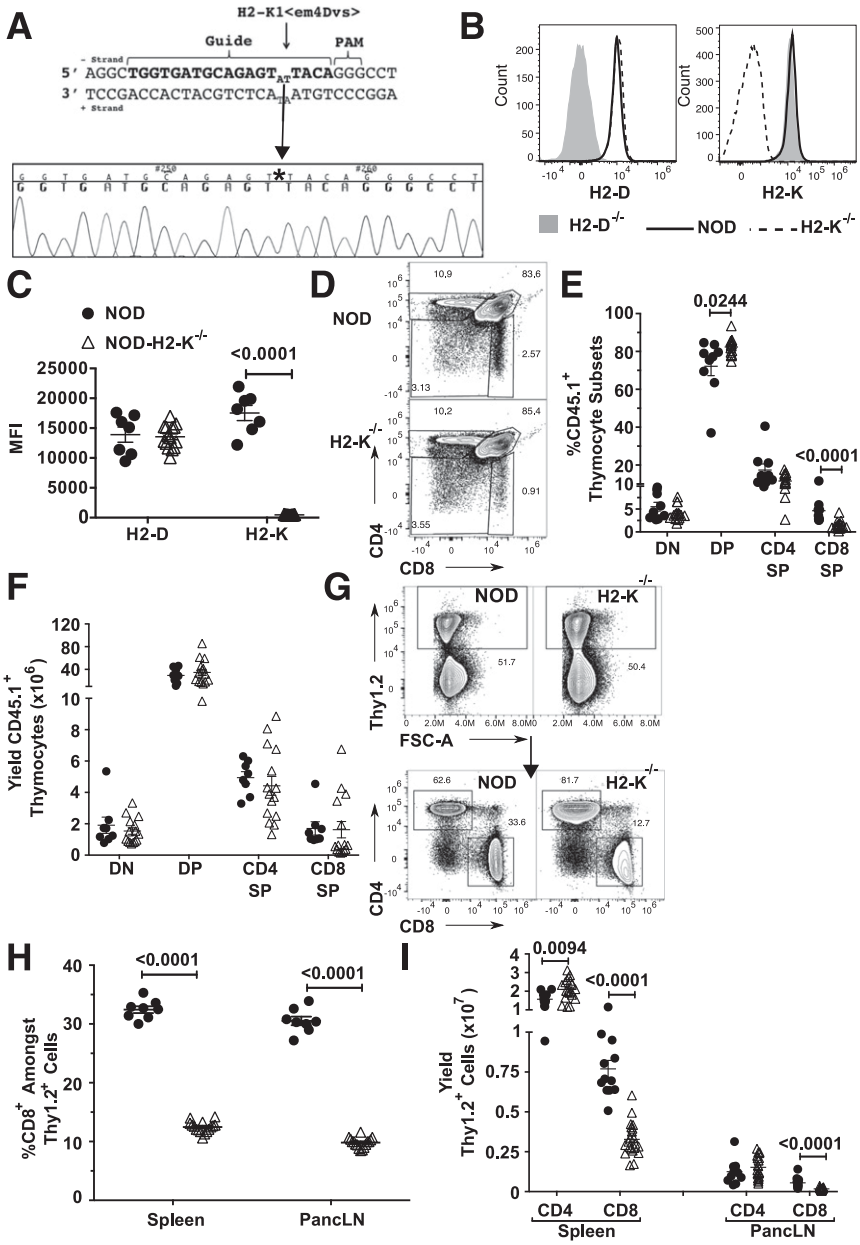

Figure 3—Novel direct-in-NOD H2-K knockout mouse generated with CRISPR/Cas9. *A*: Diagram (top) and sequence trace (bottom) showing guide sequence (bold) and protospacer adjacent motif (PAM) site within exon 3 of *H2-K1*^{d} used to generate NOD-H2-K$^{-/-}$ mice (officially designated NOD/ShiLtDvs-H2-K1$^{<em4Dvs>}$/Dvs). The subscript nucleotides represent the H2-K1<em4Dvs> mutation that is denoted with an asterisk on the sequence trace where those nucleotides are missing. *B*: Representative flow cytometry histogram showing expression of H2-D and H2-K on the cell surface of splenic B cells in comparison of 10- to 15-week-old female NOD, NOD-H2-D$^{-/-}$, and NOD-H2-K$^{-/-}$ mice. *C*: Quantification of the mean fluorescence intensity (MFI) of H2-D and H2-K antibody staining on splenic B cells (showing mean ± SEM). Individual mice are plotted, and there are 7–15 mice per group combined from two experiments. *D*: Representative flow cytometry showing CD4 vs. CD8 of gated CD45.1^{+} thymocytes in comparison of 10- to 15-week-old female NOD and NOD-H2-K$^{-/-}$ mice. *E* and *F*: Quantification of percentage (*E*) and yield (*F*) of CD45.1^{+} thymic subsets (DN, double negative; DP, double positive; SP, single positive) (showing mean ± SEM, using 8–15 mice per group combined from five experiments). *G*: Representative flow cytometry showing among splenocytes Thy1.2 vs. FSC-A (top) and Thy1.2-gated CD4 vs. CD8 (bottom) from 10- to 15-week-old female mice. *H* and *I*: Percent CD8^{+} among Thy1.2-gated cells (*H*) and yield (*I*) of spleen and PancLN CD4^{+} and CD8^{+} T cells. Showing mean ± SEM, 8–16 mice per group, combined from six experiments.

mutation, we crossed NOD-A2 and NOD-B39 mice with the newly created NOD-cMHCI$^{-/-}$ line (collectively referred to hereafter as NOD-cMHCI$^{-/-}$-HLA mice). Like their earlier NOD.β2m$^{-/-}$ counterparts, NOD-cMHCI$^{-/-}$ mice carrying A2-encoding (Fig. 6*A*) or B39-encoding (Fig. 6*B*) transgenes have CD8^{+} T cells. Also, similar to the earlier NOD.β2m$^{-/-}$ platform, NOD-cMHCI$^{-/-}$-HLA mice express their respective HLA transgenes but not murine H2-D or H2-K class I molecules (Fig. 6*C* and *E*). However, unlike their NOD.β2m$^{-/-}$ counterparts, NOD-cMHCI$^{-/-}$-A2 and NOD-cMHCI$^{-/-}$-B39

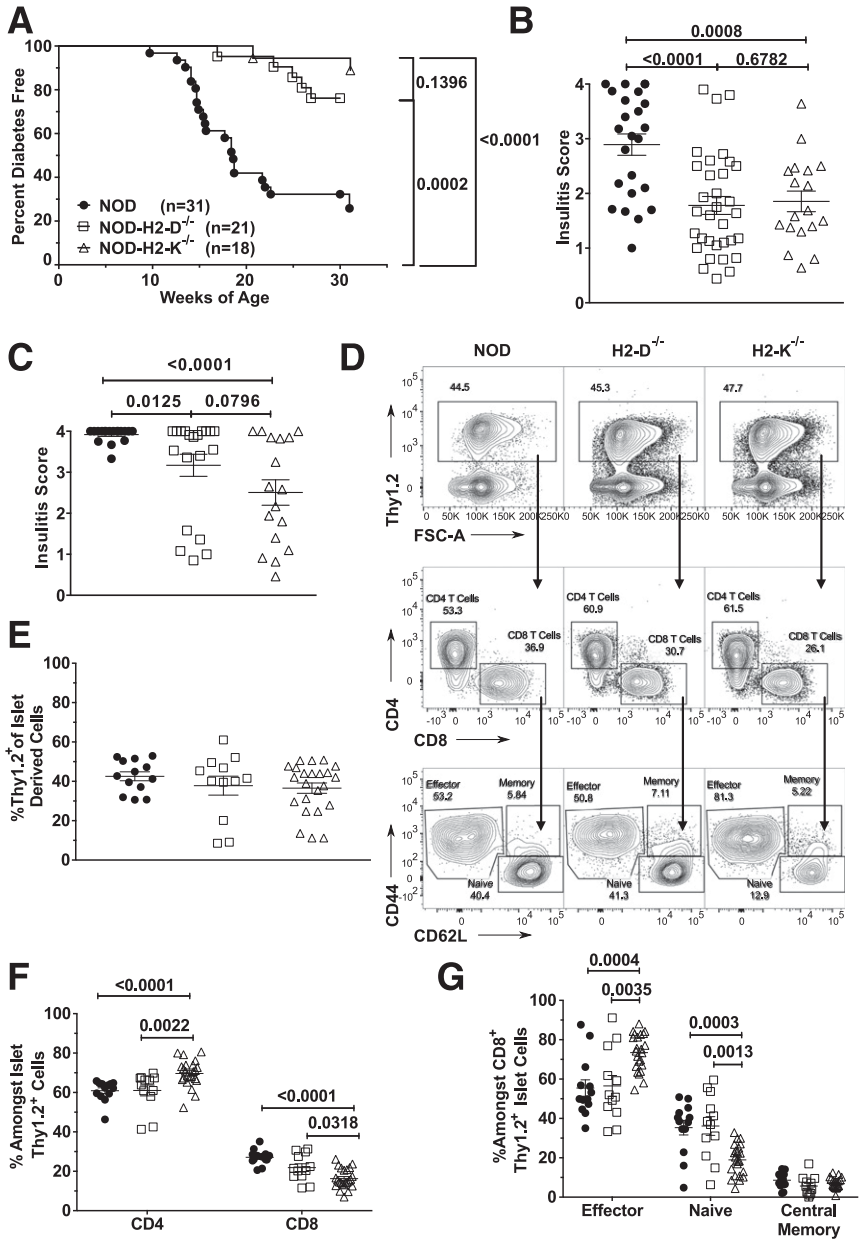

Figure 4—H2-D$^{-/-}$ and H2-K$^{-/-}$ NOD mice have decreased diabetes and insulitis. *A*: T1D incidence curves for NOD, NOD-H2-D$^{-/-}$, and NOD-H2-K$^{-/-}$ female mice. NOD is combined from two independent cohorts of 15 and 16 mice, respectively. *B*: Mean insulitis score of 10- to 15-week-old mice. *C*: Mean insulitis score of mice after 30 weeks of age, with diabetic mice automatically receiving a score of 4. *D*: Representative flow cytometry of NOD, NOD-H2-D$^{-/-}$, and NOD-H2-K$^{-/-}$ showing Thy1.2 among islet-infiltrating cells (top), CD4 vs. CD8 among gated T cells (middle), and CD44 vs. CD62L among gated islet CD8$^+$ T cells (bottom). *E–G*: Quantification of percent Thy1.2$^+$ among islet-infiltrating cells (*E*), CD4 and CD8 among islet Thy1.2$^+$ cells (*F*), and percent CD44$^+$ CD62L$^-$ effector, CD44$^-$ CD62L$^+$ naïve, and CD44$^+$ CD62L$^+$ central memory CD8$^+$ T cells (*G*), showing NOD vs. NOD-H2-D$^{-/-}$ vs. NOD-H2-K$^{-/-}$ mice. H2-K$^{-/-}$ data include eight mice from the other two H2-K$^{-/-}$ lines described in Supplementary Fig. 1.

mice express nonclassical CD1d and Qa-2 (although for unknown reasons at different levels in the transgenics [Supplementary Fig. 3]) class I molecules (Fig. 6*F* and *G*). One functional consequence of this is that NOD-cMHCI$^{-/-}$-HLA class I mice have CD1d-restricted natural killer (NK)T cells (Fig. 6*H* and *I*), a population whose therapeutic expansion could provide a means for T1D inhibition (42–44). Finally, T1D development and insulitis in both NOD-cMHCI$^{-/-}$-A2 and NOD-cMHCI$^{-/-}$-B39 mice were highly penetrant (Fig. 6*J* and *K*).

Next, we determined whether FcRn functionality was restored in NOD-cMHCI$^{-/-}$-HLA class I mice. NOD, NOD.β2m$^{-/-}$-A2, and NOD-cMHCI$^{-/-}$-A2 mice were injected with mouse trinitrophenol-specific antibody 1B7.11 (Fig. 6*L*) or humanized Herceptin IgG1 antibody (Fig. 6*M*). As expected, murine 1B7.11 antibody was cleared within a week

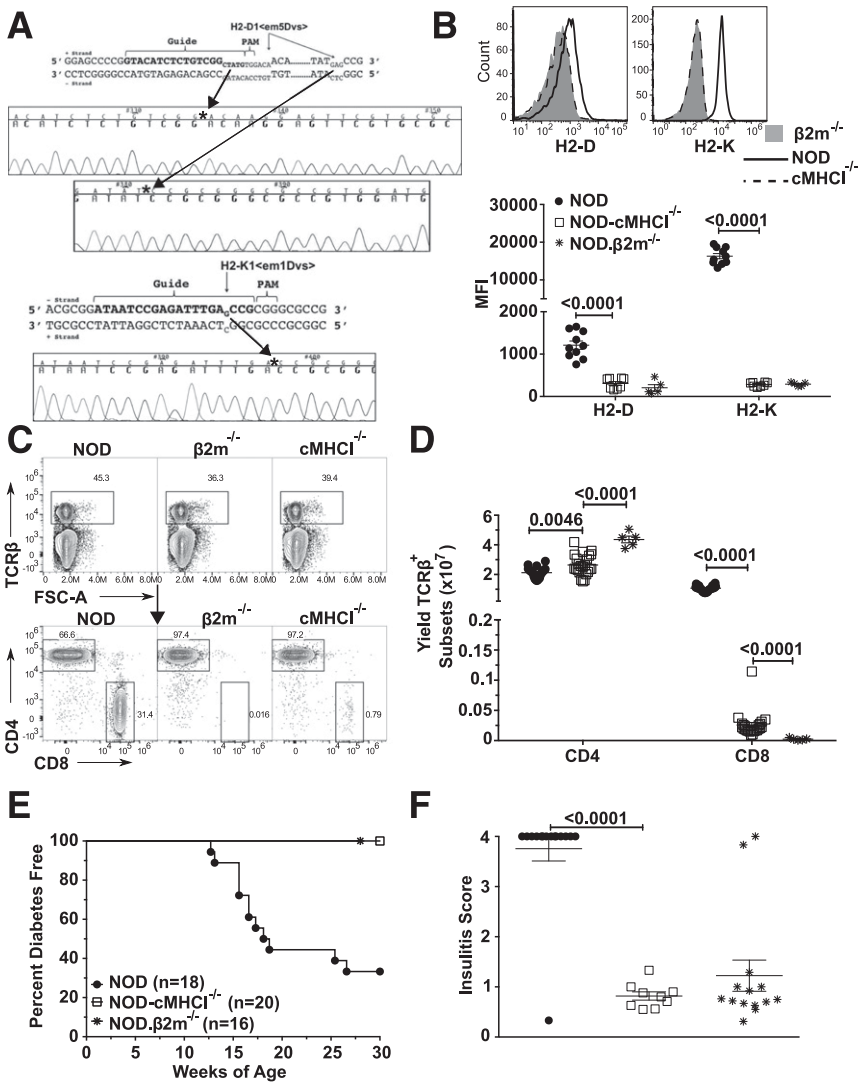

Figure 5—Novel direct-in-NOD H2-D/H2-K double knockout mice generated by CRISPR/Cas9. *A*: Diagram and sequencing traces showing location of guides, protospacer adjacent motif (PAM) sites, and mutations in exon 2 of *H2-D1*^{b} (top) and *H2-K1*^{d} (bottom). Guide sequence is in boldface type, and mutations are marked by subscripted nucleotides and marked on the sequencing trace with an asterisk. Strain officially designated NOD/ShiLtDvs-H2-K1$^{<em1Dvs>}$ H2-D1$^{<em5Dvs>}$/Dvs. *B*: Representative flow cytometry histogram (top) showing expression of H2-D and H2-K on the surface of splenic B cells in comparison of 10-week-old female NOD, NOD.β2m$^{-/-}$, and NOD-cMHCI$^{-/-}$ mice. Quantification of the mean fluorescence intensity (MFI) of H2-D and H2-K antibody staining on splenic B cells (showing mean ± SEM) (bottom). Results from individual mice are plotted and are combined from two independent experiments. There are 5–10 mice per group combined from two experiments. *C*: Representative flow cytometry showing among splenocytes TCRβ vs. FSC-A (top) and TCRβ-gated CD4 vs. CD8 (bottom) from 10-week-old female mice. *D*: Yield of splenic CD4^{+} and CD8^{+} T cells (showing mean ± SEM, 5–23 mice per group, combined from five experiments). *E*: T1D incidence comparing NOD, NOD-cMHCI$^{-/-}$, and NOD.β2m$^{-/-}$ female mice. *F*: Mean insulitis score at end of incidence showing 9–15 mice per group, with diabetic mice receiving a score of 4.

in NOD.β2m$^{-/-}$-A2 mice (Fig. 6*L*). NOD-cMHCI$^{-/-}$-A2 and NOD mice both retained detectable 1B7.11 antibody out to 30 days postinjection (Fig. 6*L*). Injected Herceptin was rapidly cleared in NOD.β2m$^{-/-}$-A2 mice but was retained at detectable levels out to 30 days in both NOD and NOD-cMHCI$^{-/-}$-A2 mice (Fig. 6*M*). These data indicate that NOD-cMHCI$^{-/-}$-HLA mice retain FcRn functionality.

Creation of NOD-cMHCI/II$^{-/-}$ Mice

Further advancement of humanized NOD models would incorporate relevant combinations of both HLA class I and II susceptibility alleles. Toward this end, we generated NOD mice completely lacking in expression of classical murine MHC molecules (NOD-cMHCI/II$^{-/-}$ mice) by CRISPR/Cas9 targeting exon 2 of *H2-Ab1*^{g7} in the NOD-cMHCI$^{-/-}$ stock (Fig. 7*A*). This resulted in a 181-bp deletion within exon 2 of *H2-Ab1*^{g7} (Fig. 7*B*). As expected, NOD-cMHCI/II$^{-/-}$ mice lack expression of H2-A^{g7}, H2-K, and H2-D (Fig. 7*C* and *D*). Thy1.2^{+} cells were reduced to ∼12% of total splenocytes in NOD-cMHCI/II$^{-/-}$ mice (Fig. 7*E* and *F*). Among residual Thy1.2^{+} cells, TCRαβ^{+} cells were reduced to 60%, with a concomitant increase in the percentage of TCRγδ cells (Fig. 7*G* and *H*). Among residual TCRαβ^{+} cells, the yield of CD4^{+} T cells was drastically reduced compared

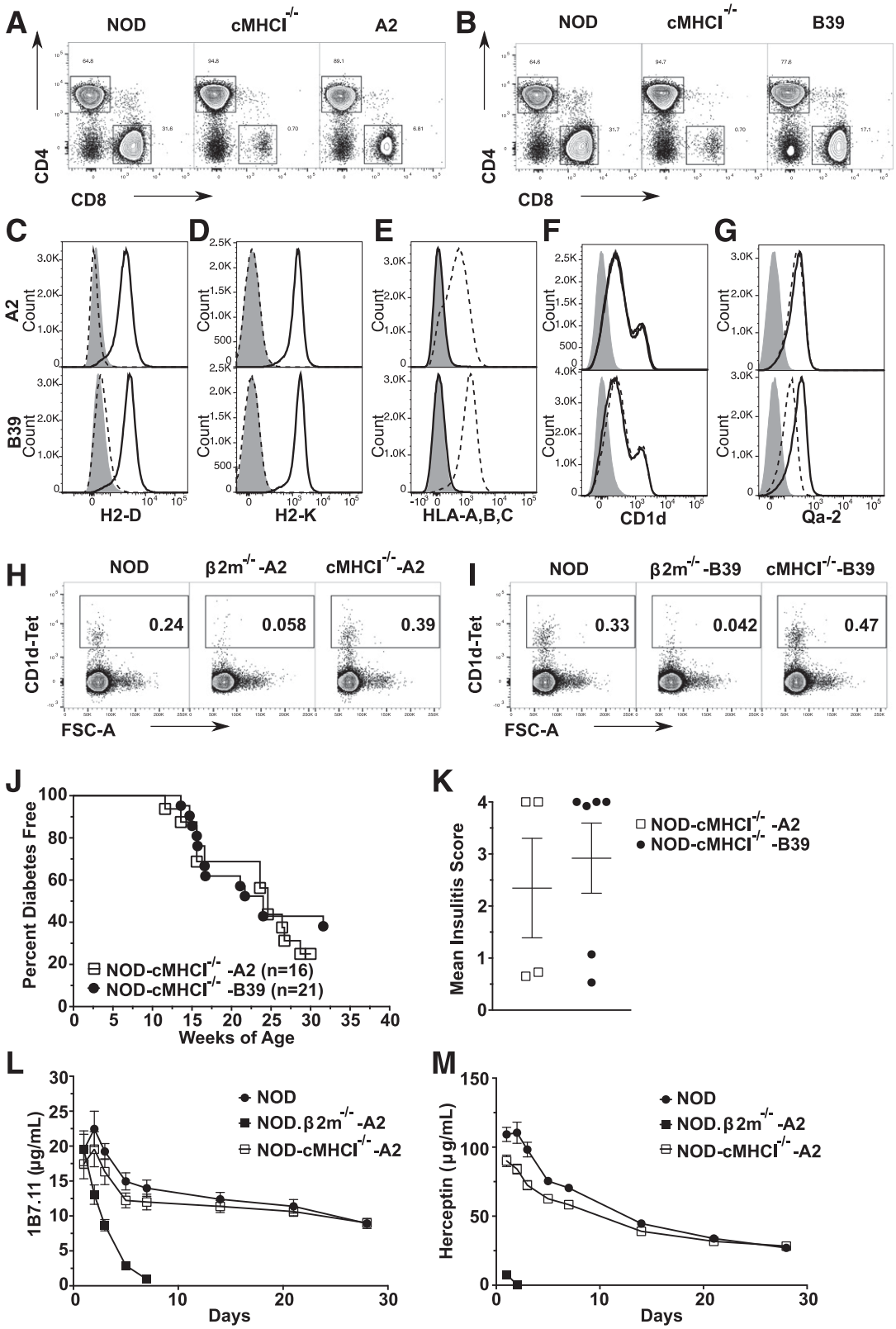

Figure 6—Novel NOD-cMHC1$^{-/-}$-HLA mice retain nonclassical MHC I, NKT cells, and FcRn functionality. A2- or B39-expressing transgenes were crossed into NOD-cMHCI$^{-/-}$ mice to generate the NOD-cMHCI$^{-/-}$-A2 (official designation NOD/ShiLtDvs-H2-K1$^{<em1Dvs>}$ H2-D1$^{<em5Dvs>}$ Tg(HLA-A/H2-D/B2M)1Dvs/Dvs) and NOD-cMHCI$^{-/-}$-B39 stocks [official designation NOD/ShiLtDvs-H2-K1$^{<em1Dvs>}$ H2-D1$^{<em5Dvs>}$ Tg(HLA-B39/H2-D/B2M)2Dvs/Dvs]. *A* and *B*: Representative spleen flow cytometry of gated TCRβ^{+} cells showing a comparison of CD4 vs. CD8 T-cell subset levels in NOD-cMHCI$^{-/-}$-A2 (*A*) or NOD-cMHCI$^{-/-}$-B39 (*B*) with NOD and NOD-cMHCI$^{-/-}$ mice. Data are representative of at least 10 mice per group examined from 8 to 20 weeks of age across three separate experiments. *C–F*: Representative histograms showing H2-D (*C*), H2-K (*D*), HLA class I (*E*), and CD1d (*F*) expression on gated splenic B cells from NOD (solid line), NOD-cMHCI$^{-/-}$-HLA-A2 or -B39 (dashed line),

with both NOD and NOD-cMHCI$^{-/-}$ mice (Supplementary Fig. 4A and Fig. 7*I*). The yield of CD8$^+$ T cells was reduced compared with NOD mice but expanded compared with NOD-cMHCI$^{-/-}$ mice (Supplementary Fig. 4A and Fig. 7*I*). CD4$^+$ and CD8$^+$ double-negative (Supplementary Fig. 4A) and NKT cells (Supplementary Fig. 4*B*) were both slightly expanded in NOD-cMHCI/II$^{-/-}$ mice in comparison with NOD and NOD-cMHCI$^{-/-}$ mice (Fig. 7*I*). Finally, when examined at 9–12 weeks of age, NOD-cMHCI/II$^{-/-}$ mice were virtually free of insulitis (Fig. 7*J*).

DISCUSSION

"Humanization" of NOD mice allowing expression of chosen HLA combinations has potential to facilitate the mechanistic analysis and development of clinically translatable T1D interventions based on individualized human genetic configurations. Toward that goal, our earlier work described NOD mice expressing the common T1D-associated human HLA-A*02:01 class I allele (21,45). We recently further advanced these resources (31) by transgenically introducing the T1D-susceptibility HLA-B*39:06 class I variant (12,17–19) into NOD mice. While a relatively low abundance allele, the human B9 class I variant supports aggressive early-onset T1D (15,16) seemingly independent of HLA class II effects (12). The continued expansion of HLA susceptibility alleles in NOD mice is essential for improving the ability to use mouse models to test therapeutics for genetically diverse T1D patient populations, as a therapy that may work with the common HLA-A2 allele in place may not be sufficient for the earlier-onset disease associated with HLA-B39 (15,16). We should note that not all HLA class I alleles are capable of supporting T1D in NOD mice, as transgenic expression of HLA-B27 actually inhibits disease development (45).

In the course of these studies, we generated NOD-H2-D$^{-/-}$ and NOD-H2-K$^{-/-}$ mice, enabling assessment of the individual contributions of these two genes to T1D development. The lack of either class I variant decreased T1D development, indicating a requirement for both H2-D– and H2-K–restricted antigens in disease pathogenesis. Initial analysis indicates that islet-infiltrating CD8$^+$ T cells in H2-K$^{-/-}$ mice have a more activated phenotype than in NOD or NOD-H2-D$^{-/-}$ mice. It is currently unknown why, while proportionally increased, islet-effector CD8$^+$ T cells in NOD-H2-K$^{-/-}$ mice appear to have dampened pathogenic activity. Work is currently underway to determine specific T-cell populations present and absent within each of these new strains and how they lead to the seeming discordance between effector status versus insulitis levels.

Our previous-generation NOD HLA-humanized models are hampered by the reliance on the *β2m*$^{-/-}$ mutation to eliminate murine MHC class I expression. β2m plays important roles in immune function beyond stabilizing H2-K and H2-D molecules on the cell surface. The NOD-cMHCI$^{-/-}$-A2 and NOD-cMHCI$^{-/-}$-B39 models described herein retain nonclassical MHC I molecules as evidenced by CD1d and Qa-2 expression (Fig. 6). We should note that while NOD-cMHCI$^{-/-}$-A2 and NOD-cMHCI$^{-/-}$-B39 mice both express Qa-2, they do so at lower levels than in NOD controls (Supplementary Fig. 3). This diminished Qa-2 expression is resultant not from ablation of murine class I molecules but, rather, for currently unknown reasons, from the presence of the human A2 or B39 variants. Owing to the association of B39 with early onset of T1D in humans (15,16), we were surprised at the low level of disease in first-generation NOD.β2m$^{-/-}$-B39 mice (31). Interestingly, more robust T1D development was observed when HLA-B39 was expressed in NOD-cMHCI$^{-/-}$ mice compared to when the same transgene was paired with an ablated β2m molecule (31). Both incidence studies were carried out at The Jackson Laboratory in the same vivarium. This suggests there may be a significant contribution, or contributions, of nonclassical MHC I molecules to T1D development in the context of HLA-B39–restricted pathogenic CD8$^+$ T cells. This might include an ability of Qa1 to modulate NK cell activity (46). Previous studies found that T1D development is exacerbated in CD1d$^{-/-}$ NOD mice (47). Thus, failure to express the nonclassical CD1d MHC class I molecule is unlikely to explain the lower T1D penetrance in NOD.β2m$^{-/-}$-B39 than in NOD-cMHCI$^{-/-}$-B39 mice. However, we cannot yet rule out that a CD1d-restricted NKT cell population in NOD-MHCI$^{-/-}$-HLA mice takes on a more pathogenic phenotype (48). Polymorphic genes in the congenic region surrounding *β2m* may contribute to decreased disease penetrance in NOD.β2m$^{-/-}$-HLA mice. This possible bystander-gene effect is avoided in NOD-cMHCI$^{-/-}$-HLA mice. Finally, another important feature of the reported HLA-humanized NOD direct–murine MHC knockout mice is that they retain FcRn functionality, allowing them to be used to test potential antibody- and serum albumin–based T1D interventions.

and NOD.β2m$^{-/-}$-HLA (shaded [*C* and *F*]) or NOD.β2m$^{-/-}$ (shaded [*D* and *E*]) mice. *G*: Representative histograms showing Qa-2 expression on gated splenic CD4$^+$ T cells from NOD (solid line), NOD.β2m$^{-/-}$-HLA (shaded line), and NOD-cMHCI$^{-/-}$-HLA (dashed line) mice. *H* and *I*: Representative flow cytometry showing staining of gated splenic TCRβ$^+$ cells with a CD1d-α-GalCer tetramer (Cd1d-Tet) vs. FSC-A comparing NOD, NOD.β2m$^{-/-}$-A2, and NOD-cMHCI$^{-/-}$-A2 (*H*) or NOD.β2m$^{-/-}$-B39 and NOD-cMHCI$^{-/-}$-B39 (*I*). T1D incidence (*J*) and end-of-incidence survivor insulitis (*K*) for female NOD-cMHCI$^{-/-}$-A2 and NOD-cMHCI$^{-/-}$-B39 mice. *L* and *M*: NOD, NOD.β2m$^{-/-}$-A2, and NOD-cMHCI$^{-/-}$-A2 mice were injected on day 0 with mouse IgG1 (1B7.11) (*L*) and humanized IgG1 (Herceptin) (*M*) (10 mg/kg and 5 mg/kg [0.1 mL/20 g body wt], respectively). Blood was obtained on days 1, 2, 3, 5, 7, 14, 21, and 28 after injection. Plasma was frozen at −20°C until the end of the study. Data are plotted as mean ± SEM of remaining antibody detectable in the blood. Data for NOD.β2m$^{-/-}$-A2 mice on days 14, 21, and 28 (1B7.11) and day 3, 5, 7, 14, 21, and 28 (Herceptin) were below the detection limit of the ELISA. There were 8–10 mice per group per time point.

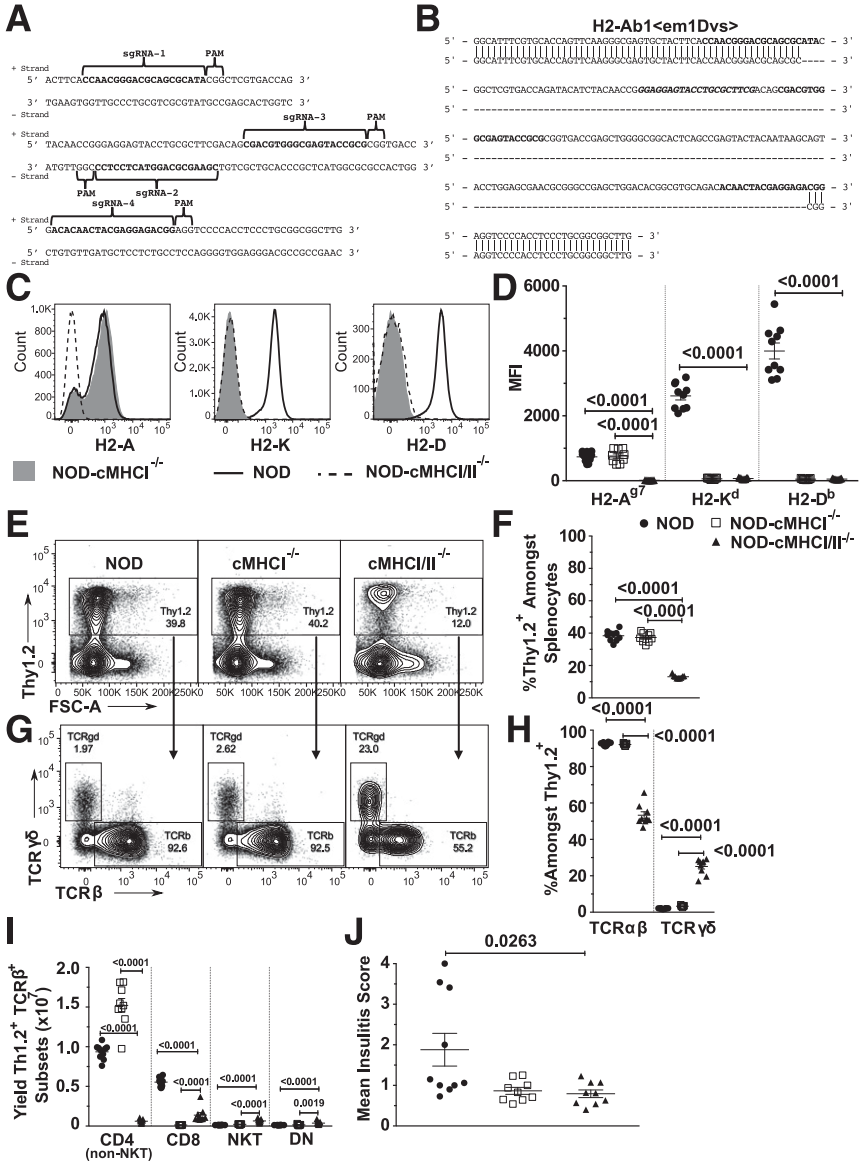

Figure 7—Novel direct-in-NOD-cMHCI/II$^{-/-}$ mice. *A*: Diagram showing single guide RNA (sgRNA) (boldface type) and protospacer adjacent motif (PAM) sites within exon 2 of *H2-Ab1*^{g7}. *B*: Alignment diagram showing location of a 181-bp deletion within exon 2 of *H2-Ab1* with guide sites listed in bold. Resultant NOD-cMHCI/II$^{-/-}$ mice officially designated NOD/ShiLtDvs-H2-K1$^{<em1Dvs>}$ H2-Ab1$^{<em1Dvs>}$ H2-D1$^{<em5Dvs>}$/Dvs. *C*: Representative flow cytometry panels showing H2-A, H2-K, and H2-D expression on gated splenic B cells. *D*: Quantification of mean fluorescence intensity (MFI) antibody staining for each MHC in comparison of NOD and NOD-cMHCI/II$^{-/-}$ mice. *E*: Representative flow cytometry panel showing percent Thy1.2$^+$ among splenocytes. *F*: Quantification of percent Thy1.2$^+$ cells comparing NOD, NOD-cMHCI$^{-/-}$, and NOD-cMHCI/II$^{-/-}$ mice. Data are combined from two experiments showing 9–10 female mice per group at 9–12 weeks of age. *G*: Representative flow cytometry panel showing percent TCRγδ vs. TCRβ among Thy1.2$^+$ cells. *H*: Quantification of percent TCRαβ vs. TCRγδ comparing NOD, NOD-cMHCI$^{-/-}$, and NOD-cMHCI/II$^{-/-}$ mice. *I*: Quantification of the yield of CD4$^+$ (CD1d-α-GalCer$^-$), CD8$^+$, NKT (CD4$^+$ and CD4$^-$ CD1d-α-GalCer$^+$), and CD4$^-$CD8$^-$ Thy1.2$^+$ TCRβ$^+$ T cells. DN, double negative. *J*: Mean insulitis score at 9–12 weeks of age comparing NOD and NOD-cMHCI/II$^{-/-}$ mice.

While the NOD-cMHCI$^{-/-}$-A2 and NOD-cMHCI$^{-/-}$-B39 models described here are improvements on the β2m$^{-/-}$ varieties, they are an intermediate step to full HLA I and II humanization, as they retain the murine H2-A^{g7} T1D susceptibility molecule. In their current state, NOD-cMHCI$^{-/-}$-A2 and NOD-cMHCI$^{-/-}$-B39 mice can serve to identify β-cell autoantigens presented by these human class I antigens to diabetogenic CD8$^+$ T cells and to test therapies that may attenuate such pathogenic effectors. These models may be improved by replacing murine H2-A^{g7} with human HLA class II transgenes. Toward this end, the NOD-cMHCI/II$^{-/-}$ mice described herein are the ideal platform for introducing any combination of HLA class I– and II–encoding transgenes. In this manner, flexible models can be generated for subpopulations of T1D patients expressing various HLA class I and II allelic combinations. We were surprised that in the absence of all classical MHC molecules, T cells still constituted ~12% of splenocytes in

NOD-cMHCI/II$^{-/-}$ mice. While we cannot completely rule out nonclassical H2-Aα/Eβ heterodimers forming in this model, to date we have been unable to detect them via available MHC II–reactive antibodies (AMS32.1, M5/114, AF6-120, 10-2.16, and 17-3-3). We speculate that in the absence of classical MHC molecules, T cells selected on nonclassical MHC molecules have space to expand in these new models. These may include type II NKT cells, which are not detected by CD1d-α-GalCer tetramers; MR1-restricted MAIT cells; and other class Ib–selected T cells (49). Additionally, CD90 (with antigen-presenting cell costimulation) can trigger T-cell proliferation in the absence of TCR engagement (50). Thus, T cells may undergo nonclassical CD90-based selection/homeostatic expansion in NOD-cMHCI/II$^{-/-}$ mice. Therefore, in addition to its utility in generating new models with differing HLA class I and II allelic combinations, we posit that NOD-cMHCI/II$^{-/-}$ mice may be useful in studying nonclassically selected T cells.

Acknowledgments. The authors thank The Jackson Laboratory's Genome Technologies group, Genetic Engineering Technologies group, Flow Cytometry service, Transgenic Genotyping Core, and Research Animal Facility for technical support on this project. The authors also thank Carl Stiewe and his wife, Maike Rohde, for their generous donation toward T1D research at The Jackson Laboratory, which contributed to this work.

Funding. PBS-57:CD1d tetramer was kindly provided from the National Institutes of Health (NIH) Tetramer Facility. During parts of this work, J.J.R. was supported by either National Institute of Diabetes and Digestive and Kidney Diseases (NIDDK), NIH, fellowship 1F32-DK-111078 or JDRF fellowship 3-PDF-2017-372-A-N. His research was also supported by a grant from the Diabetes Research Connection (DRC 006887 JR). This work was also partly supported by National Cancer Institute Cancer Center Support grant CA34196. Work by G.C., E.L., and C.M.L. was supported by NIH grant OD-020351-5019. J.S. is supported by F30 grant DK-103368 and by National Institute of General Medical Sciences grant T32 GM007288. T.P.D. is supported by NIDDK, NIH, grants R01-DK-064315, DK-094327, and AI-119225 and by a grant from the American Diabetes Association (1-16-IBS-069). T.P.D. is the Diane Belfer, Cypres & Endelson Families Faculty Scholar in Diabetes Research. D.V.S. is supported by NIDDK, NIH, grants DK-46266 and DK-95735 and by NIH Office of Director grant OD-020351-5022. National Cancer Institute, NIH, grant P30-CA-013330 supports the Cancer Center of the Albert Einstein College of Medicine, and NIDDK, NIH, grant P60-DK-020541 supports the Diabetes Research Center of the Albert Einstein College of Medicine.

Duality of Interest. No potential conflicts of interest relevant to this article were reported.

Author Contributions. J.J.R. designed and conducted experimentation, supervised experimental effort, interpreted data, and wrote the manuscript. I.S., E.L., K.H., and J.A. conducted experimentation. J.R. designed and conducted experimentation. G.C. designed and conducted experimentation and interpreted data. R.S.M. analyzed NOD/ShiLtDvs gene sequences and designed targeted CRISPR/Cas9 guides. Y.-G.C. and D.R. contributed to data interpretation and experimental conception. C.M.L. contributed to experimental conception. J.S. and T.P.D. generated the B39/HHD transgene. D.V.S. contributed to study conception, supervised experimental effort, and contributed to writing of the manuscript. D.V.S. is the guarantor of this work and, as such, had full access to all the data in the study and takes responsibility for the integrity of the data and the accuracy of the data analysis.

Prior Presentation. Parts of this study were presented in abstract form at the 77th Scientific Sessions of the American Diabetes Association, San Diego, CA, 9–13 June 2017.

References

1. Chaparro RJ, Dilorenzo TP. An update on the use of NOD mice to study autoimmune (type 1) diabetes. Expert Rev Clin Immunol 2010;6:939–955
2. Atkinson MA, Leiter EH. The NOD mouse model of type 1 diabetes: as good as it gets? Nat Med 1999;5:601–604
3. Serreze DV, Niens M, Kulik J, DiLorenzo TP. Bridging mice to men: using HLA transgenic mice to enhance the future prediction and prevention of autoimmune type 1 diabetes in humans. Methods Mol Biol 2016;1438:137–151
4. Serreze DV, Marron MP, Dilorenzo TP. "Humanized" HLA transgenic NOD mice to identify pancreatic beta cell autoantigens of potential clinical relevance to type 1 diabetes. Ann N Y Acad Sci 2007;1103:103–111
5. Noble JA, Erlich HA. Genetics of type 1 diabetes. Cold Spring Harb Perspect Med 2012;2:a007732
6. Pociot F, Akolkar B, Concannon P, et al. Genetics of type 1 diabetes: what's next? Diabetes 2010;59:1561–1571
7. Todd JA, Bell JI, McDevitt HO. HLA-DQ beta gene contributes to susceptibility and resistance to insulin-dependent diabetes mellitus. Nature 1987;329:599–604
8. Tait BD, Drummond BP, Varney MD, Harrison LC. HLA-DRB1*0401 is associated with susceptibility to insulin-dependent diabetes mellitus independently of the DQB1 locus. Eur J Immunogenet 1995;22:289–297
9. Erlich H, Valdes AM, Noble J, et al.; Type 1 Diabetes Genetics Consortium. HLA DR-DQ haplotypes and genotypes and type 1 diabetes risk: analysis of the type 1 diabetes genetics consortium families. Diabetes 2008;57:1084–1092
10. Miyazaki T, Uno M, Uehira M, et al. Direct evidence for the contribution of the unique I-ANOD to the development of insulitis in non-obese diabetic mice. Nature 1990;345:722–724
11. Serreze DV, Leiter EH, Christianson GJ, Greiner D, Roopenian DC. Major histocompatibility complex class I-deficient NOD-B2mnull mice are diabetes and insulitis resistant. Diabetes 1994;43:505–509
12. Noble JA, Valdes AM, Varney MD, et al.; Type 1 Diabetes Genetics Consortium. HLA class I and genetic susceptibility to type 1 diabetes: results from the Type 1 Diabetes Genetics Consortium. Diabetes 2010;59:2972–2979
13. Nejentsev S, Howson JM, Walker NM, et al.; Wellcome Trust Case Control Consortium. Localization of type 1 diabetes susceptibility to the MHC class I genes HLA-B and HLA-A. Nature 2007;450:887–892
14. Fennessy M, Metcalfe K, Hitman GA, et al. A gene in the HLA class I region contributes to susceptibility to IDDM in the Finnish population. Childhood Diabetes in Finland (DiMe) Study Group. Diabetologia 1994;37:937–944
15. Howson JM, Walker NM, Clayton D, Todd JA; Type 1 Diabetes Genetics Consortium. Confirmation of HLA class II independent type 1 diabetes associations in the major histocompatibility complex including HLA-B and HLA-A. Diabetes Obes Metab 2009;11(Suppl. 1):31–45
16. Valdes AM, Erlich HA, Noble JA. Human leukocyte antigen class I B and C loci contribute to type 1 Diabetes (T1D) susceptibility and age at T1D onset. Hum Immunol 2005;66:301–313
17. Roark CL, Anderson KM, Simon LJ, Schuyler RP, Aubrey MT, Freed BM. Multiple HLA epitopes contribute to type 1 diabetes susceptibility. Diabetes 2014;63:323–331
18. Mikk ML, Heikkinen T, El-Amir MI, et al.; Finnish Paediatric Diabetes Register. The association of the HLA-A*24:02, B*39:01 and B*39:06 alleles with type 1 diabetes is restricted to specific HLA-DR/DQ haplotypes in Finns. HLA 2017;89:215–224
19. Mikk ML, Kiviniemi M, Laine AP, et al.; Finnish Paediatric Diabetes Register. The HLA-B*39 allele increases type 1 diabetes risk conferred by HLA-DRB1*04:04-DQB1*03:02 and HLA-DRB1*08-DQB1*04 class II haplotypes. Hum Immunol 2014;75:65–70
20. Pascolo S, Bervas N, Ure JM, Smith AG, Lemonnier FA, Pérarnau B. HLA-A2.1-restricted education and cytolytic activity of CD8(+) T lymphocytes from beta2 microglobulin (beta2m) HLA-A2.1 monochain transgenic H-2Db beta2m double knockout mice. J Exp Med 1997;185:2043–2051

21. Takaki T, Marron MP, Mathews CE, et al. HLA-A*0201-restricted T cells from humanized NOD mice recognize autoantigens of potential clinical relevance to type 1 diabetes. J Immunol 2006;176:3257–3265
22. Jarchum I, Baker JC, Yamada T, et al. In vivo cytotoxicity of insulin-specific CD8+ T-cells in HLA-A*0201 transgenic NOD mice. Diabetes 2007;56:2551–2560
23. Jarchum I, DiLorenzo TP. Ins2 deficiency augments spontaneous HLA-A*0201-restricted T cell responses to insulin. J Immunol 2010;184:658–665
24. Jarchum I, Nichol L, Trucco M, Santamaria P, DiLorenzo TP. Identification of novel IGRP epitopes targeted in type 1 diabetes patients. Clin Immunol 2008; 127:359–365
25. Mallone R, Martinuzzi E, Blancou P, et al. CD8+ T-cell responses identify beta-cell autoimmunity in human type 1 diabetes. Diabetes 2007;56:613–621
26. Unger WW, Pinkse GG, Mulder-van der Kracht S, et al. Human clonal CD8 autoreactivity to an IGRP islet epitope shared between mice and men. Ann N Y Acad Sci 2007;1103:192–195
27. Li Y, Zhou L, Li Y, et al. Identification of autoreactive CD8+ T cell responses targeting chromogranin A in humanized NOD mice and type 1 diabetes patients. Clin Immunol 2015;159:63–71
28. Ouyang Q, Standifer NE, Qin H, et al. Recognition of HLA class I-restricted beta-cell epitopes in type 1 diabetes. Diabetes 2006;55:3068–3074
29. Pinkse GG, Tysma OH, Bergen CA, et al. Autoreactive CD8 T cells associated with beta cell destruction in type 1 diabetes. Proc Natl Acad Sci U S A 2005;102: 18425–18430
30. Niens M, Grier AE, Marron M, Kay TW, Greiner DL, Serreze DV. Prevention of "Humanized" diabetogenic CD8 T-cell responses in HLA-transgenic NOD mice by a multipeptide coupled-cell approach. Diabetes 2011;60:1229–1236
31. Racine JJ, Chapman HD, Schloss J, DiLorenzo TP, Serreze DV. Novel HLA humanized NOD-mouse models for type 1 diabetes therapy development (Abstract). Diabetes 2017;66(Suppl. 1):A480
32. Roopenian DC, Akilesh S. FcRn: the neonatal Fc receptor comes of age. Nat Rev Immunol 2007;7:715–725
33. Baker K, Rath T, Pyzik M, Blumberg RS. The role of FcRn in antigen presentation. Front Immunol 2014;5:408
34. Chaudhury C, Mehnaz S, Robinson JM, et al. The major histocompatibility complex-related Fc receptor for IgG (FcRn) binds albumin and prolongs its lifespan. J Exp Med 2003;197:315–322
35. Roopenian DC, Christianson GJ, Sproule TJ, et al. The MHC class I-like IgG receptor controls perinatal IgG transport, IgG homeostasis, and fate of IgG-Fc-coupled drugs. J Immunol 2003;170:3528–3533
36. Larsen MT, Kuhlmann M, Hvam ML, Howard KA. Albumin-based drug delivery: harnessing nature to cure disease. Mol Cell Ther 2016;4:3
37. Hill JT, Demarest BL, Bisgrove BW, Su YC, Smith M, Yost HJ. Poly peak parser: method and software for identification of unknown indels using sanger sequencing of polymerase chain reaction products. Dev Dyn 2014;243:1632–1636
38. Julius MH, Herzenberg LA. Isolation of antigen-binding cells from unprimed mice: demonstration of antibody-forming cell precursor activity and correlation between precursor and secreted antibody avidities. J Exp Med 1974;140:904–920
39. Russo C, Ng AK, Pellegrino MA, Ferrone S. The monoclonal antibody CR11-351 discriminates HLA-A2 variants identified by T cells. Immunogenetics 1983;18:23–35
40. Johnson EA, Silveira P, Chapman HD, Leiter EH, Serreze DV. Inhibition of autoimmune diabetes in nonobese diabetic mice by transgenic restoration of H2-E MHC class II expression: additive, but unequal, involvement of multiple APC subtypes. J Immunol 2001;167:2404–2410
41. Serreze DV, Chapman HD, Niens M, et al. Loss of intra-islet CD20 expression may complicate efficacy of B-cell-directed type 1 diabetes therapies. Diabetes 2011; 60:2914–2921
42. Sharif S, Arreaza GA, Zucker P, et al. Activation of natural killer T cells by alpha-galactosylceramide treatment prevents the onset and recurrence of autoimmune Type 1 diabetes. Nat Med 2001;7:1057–1062
43. Wang B, Geng YB, Wang CR. CD1-restricted NK T cells protect nonobese diabetic mice from developing diabetes. J Exp Med 2001;194:313–320
44. Chen YG, Choisy-Rossi CM, Holl TM, et al. Activated NKT cells inhibit autoimmune diabetes through tolerogenic recruitment of dendritic cells to pancreatic lymph nodes. J Immunol 2005;174:1196–1204
45. Marron MP, Graser RT, Chapman HD, Serreze DV. Functional evidence for the mediation of diabetogenic T cell responses by HLA-A2.1 MHC class I molecules through transgenic expression in NOD mice. Proc Natl Acad Sci U S A 2002;99: 13753–13758
46. Vance RE, Kraft JR, Altman JD, Jensen PE, Raulet DH. Mouse CD94/NKG2A is a natural killer cell receptor for the nonclassical major histocompatibility complex (MHC) class I molecule Qa-1(b). J Exp Med 1998;188:1841–1848
47. Shi FD, Flodstrom M, Balasa B, et al. Germ line deletion of the CD1 locus exacerbates diabetes in the NOD mouse. Proc Natl Acad Sci U S A 2001;98:6777–6782
48. Simoni Y, Gautron AS, Beaudoin L, et al. NOD mice contain an elevated frequency of iNKT17 cells that exacerbate diabetes. Eur J Immunol 2011;41:3574–3585
49. Godfrey DI, Uldrich AP, McCluskey J, Rossjohn J, Moody DB. The burgeoning family of unconventional T cells. Nat Immunol 2015;16:1114–1123
50. Haeryfar SM, Al-Alwan MM, Mader JS, Rowden G, West KA, Hoskin DW. Thy-1 signaling in the context of costimulation provided by dendritic cells provides signal 1 for T cell proliferation and cytotoxic effector molecule expression, but fails to trigger delivery of the lethal hit. J Immunol 2003;171:69–77